Solution Structure of the Catalytic Domain of the Mitochondrial Protein ICT1 That Is Essential for Cell Vitality

Yoshihiro Handa[1], Yusuke Hikawa[1], Naoya Tochio[2], Hiroyuki Kogure[1], Makoto Inoue[2], Seizo Koshiba[2], Peter Güntert[3], Yusuke Inoue[1], Takanori Kigawa[2,4], Shigeyuki Yokoyama[2,5] and Nobukazu Nameki[1]*

[1]*Department of Chemistry and Chemical Biology, Graduate School of Engineering, Gunma University, 1-5-1 Tenjin-cho, Kiryu-shi, Gunma 376-8515, Japan*

[2]*RIKEN Systems and Structural Biology Center, 1-7-22 Suehiro-cho, Tsurumi, Yokohama 230-0045, Japan*

[3]*Institute of Biophysical Chemistry, Center for Biomolecular Magnetic Resonance, and Frankfurt Institute for Advanced Studies, Goethe University Frankfurt am Main, Max-von-Laue-Str. 9, 60438 Frankfurt am Main, Germany*

[4]*Department of Computational Intelligence and Systems Science, Interdisciplinary Graduate School of Science and Engineering, Tokyo Institute of Technology, Yokohama, Kanagawa 226-8502, Japan*

[5]*Department of Biophysics and Biochemistry, Graduate School of Science, University of Tokyo, Bunkyo-ku, Tokyo 113-0033, Japan*

The ICT1 protein was recently reported to be a component of the human mitoribosome and to have codon-independent peptidyl-tRNA hydrolysis activity via its conserved GGQ motif, although little is known about the detailed mechanism. Here, using NMR spectroscopy, we determined the solution structure of the catalytic domain of the mouse ICT1 protein that lacks an N-terminal mitochondrial targeting signal and an unstructured C-terminal basic-residue-rich extension, and we examined the effect of ICT1 knockdown (mediated by small interfering RNA) on mitochondria in HeLa cells using flow cytometry. The catalytic domain comprising residues 69–162 of the 206-residue full-length protein forms a structure with a β1–β2–α1–β3–α2 topology and a structural framework that resembles the structure of GGQ-containing domain 3 of class 1 release factors (RFs). Half of the structure, including the GGQ-containing loop, has essentially the same sequence and structure as those in RFs, consistent with the peptidyl-tRNA hydrolysis activity of ICT1 on the mitoribosome, which is analogous to RFs. However, the other half of the structure differs in shape from the corresponding part of RF domain 3 in that in ICT1, an α-helix (α1), instead of a β-turn, is inserted between strand β2 and strand β3. A characteristic groove formed between α1 and the three-stranded antiparallel β-sheet was identified as a putative ICT1-specific functional site by a structure-based alignment. In addition, the structured domain that recognizes stop codons in

RFs is replaced in ICT1 by a C-terminal basic-residue-rich extension. It appears that these differences are linked to a specific function of ICT1 other than the translation termination mediated by RFs. Flow cytometry analysis showed that the knockdown of ICT1 results in apoptotic cell death with a decrease in mitochondrial membrane potential and mass. In addition, cytochrome *c* oxidase activity in ICT1 knockdown cells was decreased by 35% compared to that in control cells. These results indicate that ICT1 function is essential for cell vitality and mitochondrial function.

Introduction

The ICT1 gene was originally found by a comparison of gene expressions between undifferentiated and differentiated HT29-D4 human colon carcinoma cells.[1,2] Among many differentially expressed genes, its mRNA was strongly downregulated during *in vitro* differentiation of HT29-D4 cells; thus, the gene was named ICT1 (*i*mmature *c*olon carcinoma cell *t*ranscript 1). Homologous genes are conserved not only in eukaryotes but also in bacteria, although few studies on ICT1 have so far been carried out.

According to the Pfam database generated by multiple-sequence alignments using hidden Markov models,[3] the ICT1 protein belongs to the release factor (RF)-1 family, which includes class I polypeptide chain RFs from bacteria and mitochondrial RFs (Fig. 1a). For translation termination, bacteria have two RFs, RF1 and RF2, which specifically recognize UAG/UAA and UGA/UAA stop codons, respectively, while mitochondria have mtRF1a (also called HMRF1L), which recognizes UAG/UAA stop codons. The bacterial-type RFs are composed of four domains, each of which has specific roles when bound to a ribosome for translation termination (Fig. 1b). For recognition of the stop codon, domains 2 and 4 interact with the decoding center in the small ribosomal subunit.[4,5] Domain 3 interacts with the peptidyltransferase center (PTC) of the large ribosomal subunit to trigger peptidyl-tRNA hydrolysis (PTH), which releases the nascent polypeptide chain from the P-site-bound peptidyl-tRNA. The catalysis involves a universally conserved Gly-Gly-Gln motif (the GGQ motif) in domain 3.[6,7] The interdomain space on the ribosome is bridged by domain 1. It is notable that although all ICT1 proteins have the GGQ motif, they are shorter than the RFs (Fig. 1a). The Pfam database shows that the sequence in the vicinity of the GGQ motif (~25 residues) that defines the RF-1 family can be aligned well between ICT1 proteins and RFs, whereas the other sequence regions are poorly aligned.

Comprehensive analyses of subcellular localizations using green fluorescent protein tagging have shown that the human ICT1 protein and its yeast homologue are localized in mitochondria.[8,9] The N-terminal extension that exists in all eukaryotic ICT1 proteins is a mitochondria-targeting presequence (Fig. 1a).[9,10] Recently, it has been reported that the human ICT1 protein is a component of mitochondrial ribosome (mitoribosome) and that it has PTH activity via the GGQ motif.[10] Intriguingly, unlike RFs, the PTH activity of ICT1 is codon-independent. Thus, ICT1 has been suggested to be involved in some translation process other than the translation termination process mediated by RFs.[10]

To obtain insights into the functional differences between ICT1 and RFs, we determined, using heteronuclear NMR methods, the solution structure of a truncated ICT1 protein from a mouse that lacks the N-terminal mitochondrial targeting signal and an unstructured C-terminal extension. This structured region contains the catalytic GGQ motif and thus is referred to as the catalytic domain. The determined

Fig. 1. Comparisons between ICT1 proteins and bacterial-type RFs from various organisms. (a) Schematic domain representations of RF1 family proteins: *E. coli* RF2, mouse ICT1 protein, and its *E. coli* homologue *yaeJ*. Numbering is according to the ICT1 structure determined in this study and the structure of free *E. coli* RF2 (PDB code 1GQE). (b) Structure of RF2 bound to the 70S ribosome from *T. thermophilus* (PDB code 2WH1). The ribosome structure is not drawn. Domains 1, 2, and 4 are shown in the same colors as in (a). In domain 3 containing the GGQ motif, the α-helices and the β-sheet are shown in pink and light green, respectively. (c) Structure-based sequence alignment of ICT1 proteins from various organisms (from bacteria to eukaryotes) and bacterial and mitochondrial RFs. The secondary structure elements of the ICT1 structure determined in this study and of the RF2 structure (PDB code 1GQE) are indicated. The truncation positions for the ICT1 protein used in this structural determination are marked by vertical arrows. Asterisks indicate highly conserved residues (>94%) among both ICT1 proteins and RFs. (#) Highly conserved residues among the ICT1 proteins from bacteria to eukaryotes. Alignments are as follows: purple: glycine (G); yellow: proline (P); green: small and hydrophobic amino acids (A, V, L, I, M, F, W); gray: hydroxyl and amine amino acids (S, T, N, Q); red: charged amino acids (D, E, R, K); cyan: histidine (H) and tyrosine (Y).
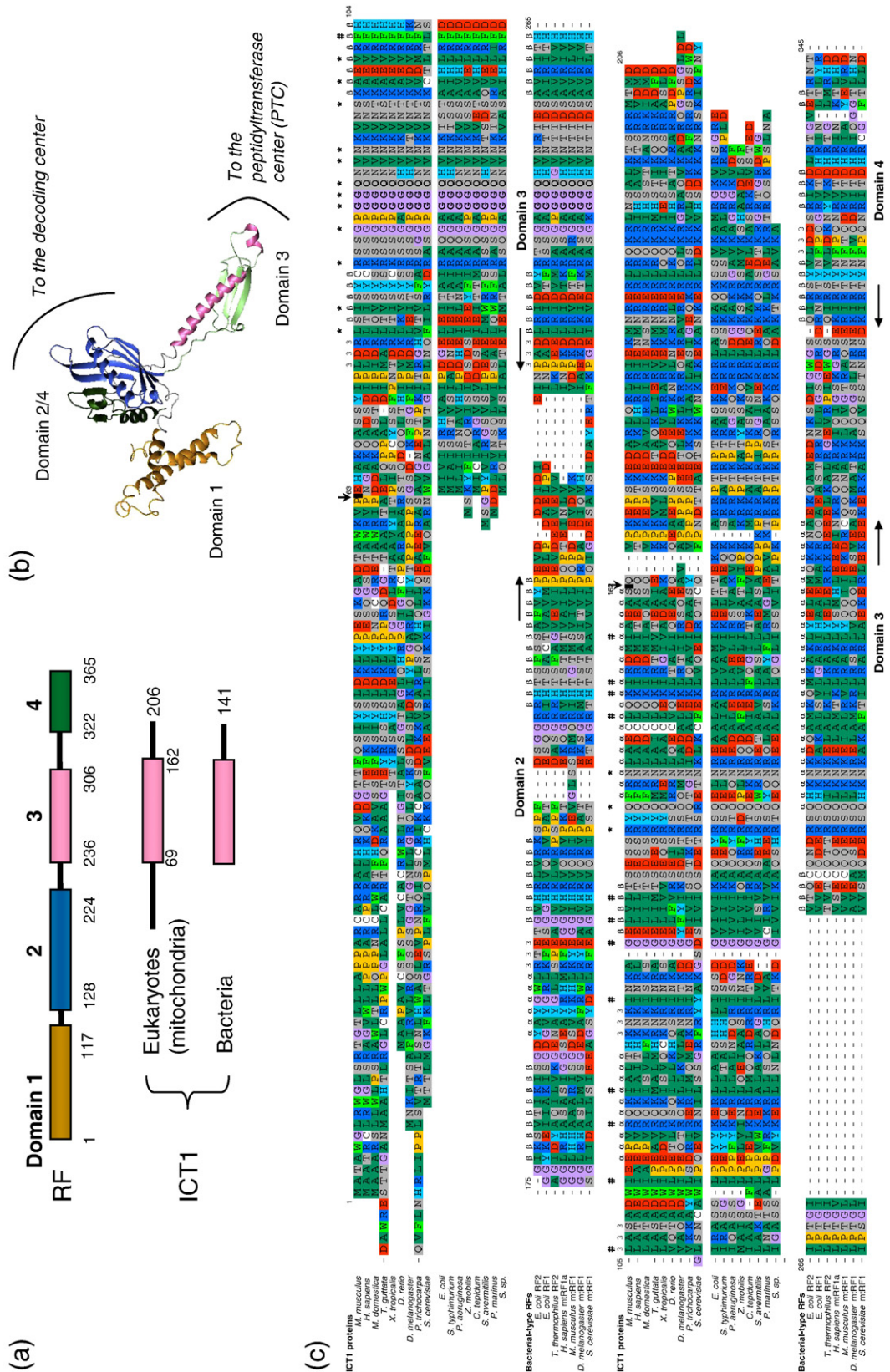
Fig. 1 (*legend on previous page*)

structure enabled structure-based alignments and detailed structural comparisons with RFs, revealing not only similarities that allow ICT1 with its PTH activity to enter into a ribosome in the same way as RFs but also key differences for discriminating between the functions of ICT1 and the functions of RFs. Furthermore, to assess the function of ICT1 in mitochondria, we performed flow cytometry (FCM) analyses using small interfering RNA (siRNA)-mediated knockdown of ICT1 in HeLa cells. The findings showed a significant contribution of ICT1 to the function of mitochondria.

Results

Protein expression

The protein encoded by the mouse ICT1 gene is composed of 206 residues (Fig. 1a).[1] We first designed a truncated protein that lacks the N-terminal 62 residues, since the N-terminal extension functions as an import signal into mitochondria.[9,10] The position of the first residue in the truncated protein corresponds to that of the first residue Met in the *Escherichia coli* ICT1 homologue (*yaeJ*) (Fig. 1c). ^{15}N-labeled and ^{13}C/^{15}N-labeled protein samples for NMR measurements were prepared by a cell-free protein expression system.[11,12] Consequently, all expressed proteins have artificial tag sequences (13 residues in total) at the N-terminus (GSSGSSG) and the C-terminus (SGPSSG), which are both derived from the expression vector. The ^{1}H,^{15}N hetero-nuclear single-quantum coherence spectrum of the ^{15}N-labeled truncated protein showed that the protein was structured, although some resonances were within a narrow region indicating a partial random-coil structure (data not shown). Thus, we also removed the C-terminal region ranging from residue 163 to residue 206, which abounds in basic residues (Fig. 1c). The resulting truncated protein (Glu63-Ser162) exhibited well-dispersed resonances (data not shown).

Resonance assignments and structure determination

For structure determination of the truncated and tagged version of the ICT1 protein, which corresponds to the catalytic domain, NMR resonances were assigned with the ^{13}C/^{15}N-labeled protein composed of 113 residues using conventional heteronuclear methods. The backbone resonance assignments were complete, with the exception of three consecutive residues (Phe144, Arg145, and Asn146) and the first three residues (GSS) and the last residue (Gly) in the N-terminal and C-terminal tag regions. Tertiary structures

Table 1. Summary of the conformational constraints and statistics of the NMR solution structure of the ICT1 protein

NOE upper distance restraints		
Intraresidual ($\lvert i-j \rvert = 0$)	358	
Medium range ($1 \le \lvert i-j \rvert \le 4$)	798	
Long range ($\lvert i-j \rvert > 4$)	448	
Total	1604	
Dihedral angle restraints (ϕ and ψ)	81	
CYANA target function value (Å^2)	1.76 ± 0.19	
Number of restraint violations		
Distance restraint violations (> 0.4 Å)	0	
Dihedral angle restraint violations ($> 3.0°$)	0	
AMBER energies (kcal/mol)		
Total	-4048 ± 105	
van der Waals	-272 ± 10	
Electrostatic	-4690 ± 109	
RMSD from ideal geometry		
Bond lengths (Å)	0.0074 ± 0.0001	
Bond angles (°)	1.87 ± 0.03	
Ramachandran plot (%)	Residues 63–162	Residues 71–81 and 98–162
Residues in most favored regions	73.5	83.4
Residues in additionally allowed regions	20.0	13.2
Residues in generously allowed regions	4.7	3.0
Residues in disallowed regions	1.8	0.5
RMSD from averaged coordinates (Å)	Residues 71–81 and 98–162	
Backbone atoms	0.30 ± 0.04	
Heavy atoms	0.72 ± 0.06	

were calculated using the CYANA software package[13,14] based on a total of 1604 nuclear Overhauser enhancement (NOE)-derived distance restraints and 81 backbone torsion-angle restraints (Table 1; Supplementary Fig. 1). A best-fit super-position of the ensemble of the 20 lowest-energy calculated conformers is shown in Fig. 2a. The root-mean-square deviation (RMSD) from the mean structure was 0.30 ± 0.04 Å for the backbone (N, C$^\alpha$, and C′) atoms and 0.72 ± 0.06 Å for all heavy (nonhydrogen) atoms in the well-ordered region of residues 71–81 and 98–162. The statistics of the structures are summarized in Table 1.

NMR results show that the structure consists of a three-stranded antiparallel β-sheet side by side with an α-helix, and an α-helix linking two β-strands with a topology of β1–β2–α1–β3–α2 (Fig. 2b). The β-sheet consists of three antiparallel β-strands (β1: residues 78–82; β2: residues 98–104; β3: residues 132–136). A 3_{10}-helical turn (3_{10}-1: residues 74–76) precedes β1. Strands β1 and β2 are connected by a disordered loop (residues 83–97), including the ^{88}GGQ^{90} residues, which is termed the GGQ loop. A structured region (residues 105–131) containing a 3_{10}-helix (3_{10}-2: residues 105–107), an α-helix (α1: residues 113–122),
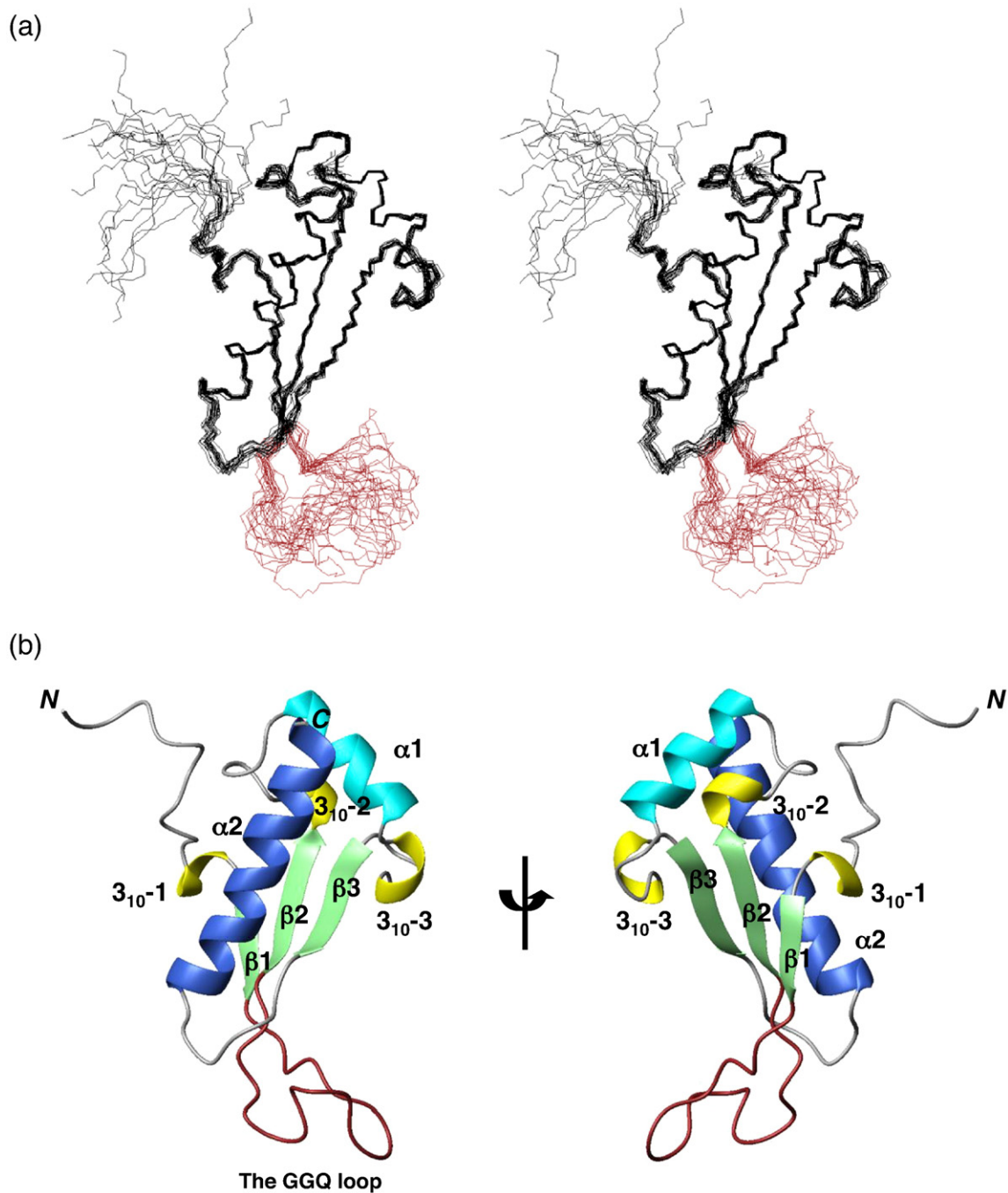
Fig. 2. Solution structure of the catalytic domain of the ICT1 protein. (a) Stereo view illustrating a trace of the backbone atoms of the 20 energy-refined conformers that represent the solution structure (residues 63–162). The GGQ loop is shown in brown. (b) Ribbon diagrams of the ICT1 structure. The orientation on the left is the same as in (a). On the right, the view is rotated by 180° around the vertical axis. The α-helices α1 and α2 are shown in blue and cyan, respectively. The 3_{10} helices, β-strands, and GGQ loop are shown in yellow, light green, and brown, respectively.

and a 3_{10}-helix (3_{10}-3: residues 124–126) is inserted between β2 and β3. Following β3, a long α-helix (α2: residues 144–162) lies on the β-sheet, crossing over α1. As a result, the structured region of the ICT1 protein ranges from Ser69 to Ser162.

Structural comparison with domain 3 of bacterial-type RFs

A comparison with the RF2 structure demonstrated that the catalytic domain of the ICT1 protein is
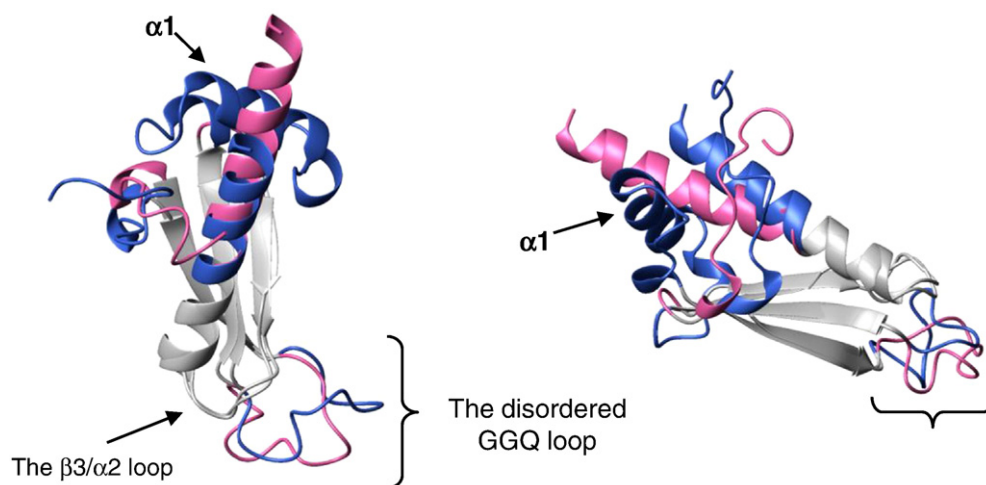
Fig. 3. Superposition of the structures of the catalytic domain of the ICT1 protein and domain 3 of free *E. coli* RF2 (PDB code 1GQE). The image on the left shows ribbon diagrams of the two structures in the same orientation as in Fig. 1a. The image on the right shows the same superposition in a different orientation. Note that the GGQ loops of both structures are disordered, as described in the text. Shown in gray are the regions used for determining the optimal superposition: residues 77–83, 97–104, and 132–150 in the ICT1 protein; residues 239–245, 259–266, and 269–287 in RF2 domain 3. The other regions of the ICT1 protein and RF2 domain 3 are shown in blue and pink, respectively. Arrows indicate the characteristic $\alpha 1$ helix and the $\beta 3/\alpha 2$ loop, as described in the text.

virtually identical in structural framework to domain 3 of RF2, which directly interacts with the PTC (Fig. 3). The RMSD between the two structures is 0.97 Å for the backbone atoms in the region, including the three-stranded β-sheet, the first half of $\alpha 2$, and the loop connecting $\beta 3$ and $\alpha 2$ (Fig. 3). The comparison also showed that the location and length (15 residues) of the GGQ loop are identical in both proteins. In the solution structures, the GGQ loop was found to be unstructured (Fig. 2a; Supplementary Fig. 1). This finding is consistent with the poor electron density for the GGQ loop in the RF crystal structures, indicating that the GGQ loop is mobile and thus disordered in the crystals.[15] Crystal structures of the 70S ribosome in complex with RF have demonstrated that the GGQ loop of bound RF adopts a fixed conformation and that the GGQ motif residues contribute directly to PTH activity (Fig. 1b).[16–18]

The only difference in structural framework between domain 3 of RF2 and the catalytic domain of ICT1 was found in the region connecting $\beta 2$ and $\beta 3$, where the former has a five-residue β-turn whereas the latter has a 10-residue α-helix ($\alpha 1$) sandwiched between the β-sheet and $\alpha 2$ (Fig. 3). The existence of the α-helix is related to the slight disagreement ($\sim 10°$) of the angle of $\alpha 2$ against the β-sheet. It is notable that this position of $\alpha 1$ does not disturb the structural framework of domain 3. Structure-based alignment revealed that this characteristic α-helix region is conserved among all of the catalytic domains of ICT1 proteins from bacteria to eukaryotes (Fig. 1c).

FCM analysis using siRNA-mediated knockdown

To assess ICT1 function in mitochondria, we downregulated ICT1 expression in HeLa cells using siRNA methods. Untreated cells (control) and cells transfected with nontargeting siRNA (si-NT) served as negative controls. The siRNA used was efficient in the knockdown of ICT1 from cells (Fig. 4a). Three

Fig. 4. Apoptotic cell death in ICT1-downregulated HeLa cells. (a) Immunoblot analysis showing ICT1 and γ-tubulin protein levels in HeLa cells harvested from a 3-day experiment. (b) Numbers of HeLa cells in standard glucose media counted at 1-day intervals. HeLa cells were untreated (Control) or transfected with nontargeting control (si-NT) or with si-ICT1. Data points show the mean of three independent experiments; bars indicate standard deviation. (c) FCM analysis of DNA content per cell cycle using PI. HeLa cells that were transfected with si-NT or si-ICT1 or treated with 50 nmol of an apoptotic inducer (staurosporine) and grown for 3 days. Cells were stained with PI and measured by FCM. Bars correspond to the sub-G_1 phase representing cells with DNA fragmentation. (d) Scatter plots of the FCM determination of the numbers of apoptotic, necrotic, and viable cells. HeLa cells were transfected with si-NT or si-ICT1 or treated with 50 nmol of staurosporine and grown for 3 days. Cells were labeled with PI and Annexin V and analyzed by FCM. Early apoptotic cells were localized in the upper left quadrant of a dot-plot graph using PI *versus* Annexin V. Results are representative of three independent experiments.

days after the addition of siRNA, a 52% reduction in cell numbers was observed in ICT1-downregulated cells compared to the si-NT control cells, indicating inhibition of cell proliferation (Fig. 4b). Similar results were obtained in human hepatoblastoma HepG2 cells (data not shown). To further examine the effects of the lack of ICT1 on cell proliferation, we performed FCM analyses of the ICT1-downregulated cells. First, to
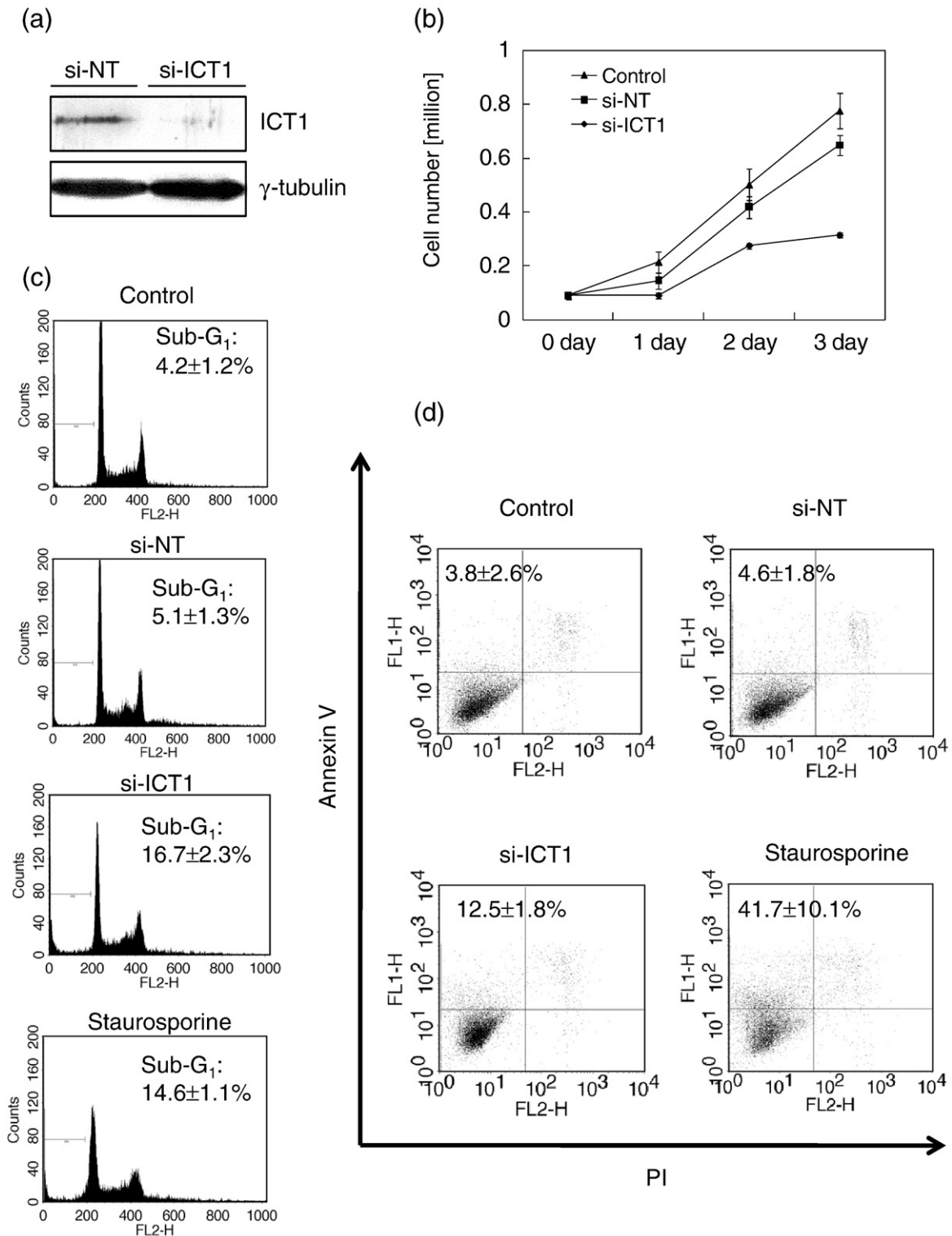

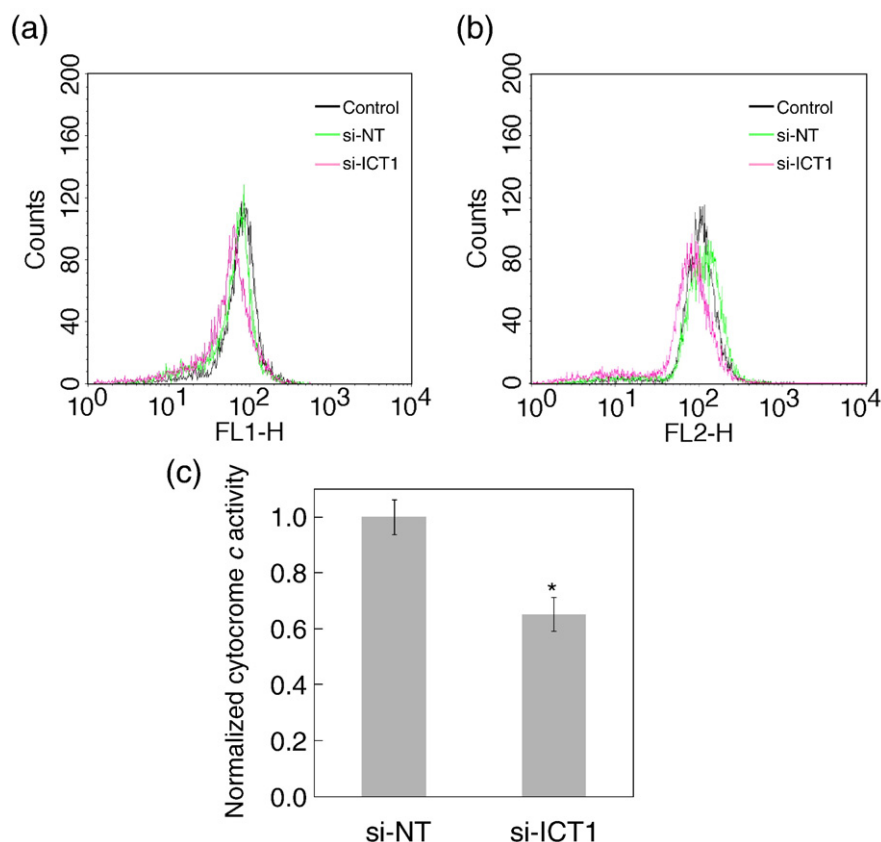**Fig. 4** (*legend on previous page*)

Fig. 5. Effects of ICT1 knockdown on mitochondria. (a) Mitochondrial membrane potential measured by FCM using MitoTracker Red CMXRos. HeLa cells were transfected with si-NT or si-ICT1 and grown for 3 days. Results are representative of three independent experiments. (b) Mitochondrial mass was measured by FCM using MitoTracker Green FM. (c) Cytochrome *c* oxidase activity. Data are presented as mean±standard deviation for three independent experiments. *$P < 0.05$.

analyze the cell cycle profile, we stained the ICT1-downregulated cells with propidium iodide (PI) after a 3-day treatment, and we counted the cell populations in each phase by FCM. FCM of cellular DNA content using PI staining revealed the distribution of cells into fractions in the sub-G_1, G_1, S, and G_2/M phases. FCM analysis showed that 17% of the ICT1-downregulated cells accumulated in the sub-G_1 phase in contrast to 5% of si-NT control cells, indicating that apoptosis occurs in the cells (Fig. 4c). Annexin V and PI stainings were performed to confirm apoptotic cell death. This staining combination enables viable, apoptotic, and necrotic cells to be distinguished.[19] As shown in Fig. 4d, 13% of the ICT1-downregulated cells were apoptotic, while only 5% of the si-NT control cells were apoptotic. An approximately 3-fold increase in apoptotic populations compared to controls has been found in similar gene knockdown experiments.[20,21] These results indicate that the lack of ICT1 results in apoptotic cell death.

To characterize mitochondrial properties in ICT1-downregulated cells, we measured changes in mitochondrial membrane potential and mass in the ICT1-downregulated cells by FCM analysis using the uptake of MitoTracker Green FM and MitoTracker Red CMXRos, respectively. Uptake of the former dye is dependent on mitochondrial mass but not mitochondrial membrane potential, whereas that of the latter has the opposite characteristic. Decreases in both mitochondrial membrane potential and mass in the ICT1-downregulated cells were observed compared to those in controls (Fig. 5a and b).

Furthermore, to examine the effects of the lack of ICT1 on mitochondrial activity, we performed a cytochrome *c* oxidase activity assay in an isolated mitochondrial fraction from ICT1-downregulated cells. The activity of cytochrome *c* oxidase was decreased by 35% compared to that in the si-NT control cells (Fig. 5c).

Discussion

In this study, we determined the solution structure of the catalytic domain of the eukaryotic ICT1 protein. Based on the structured region, the ICT1 sequence can
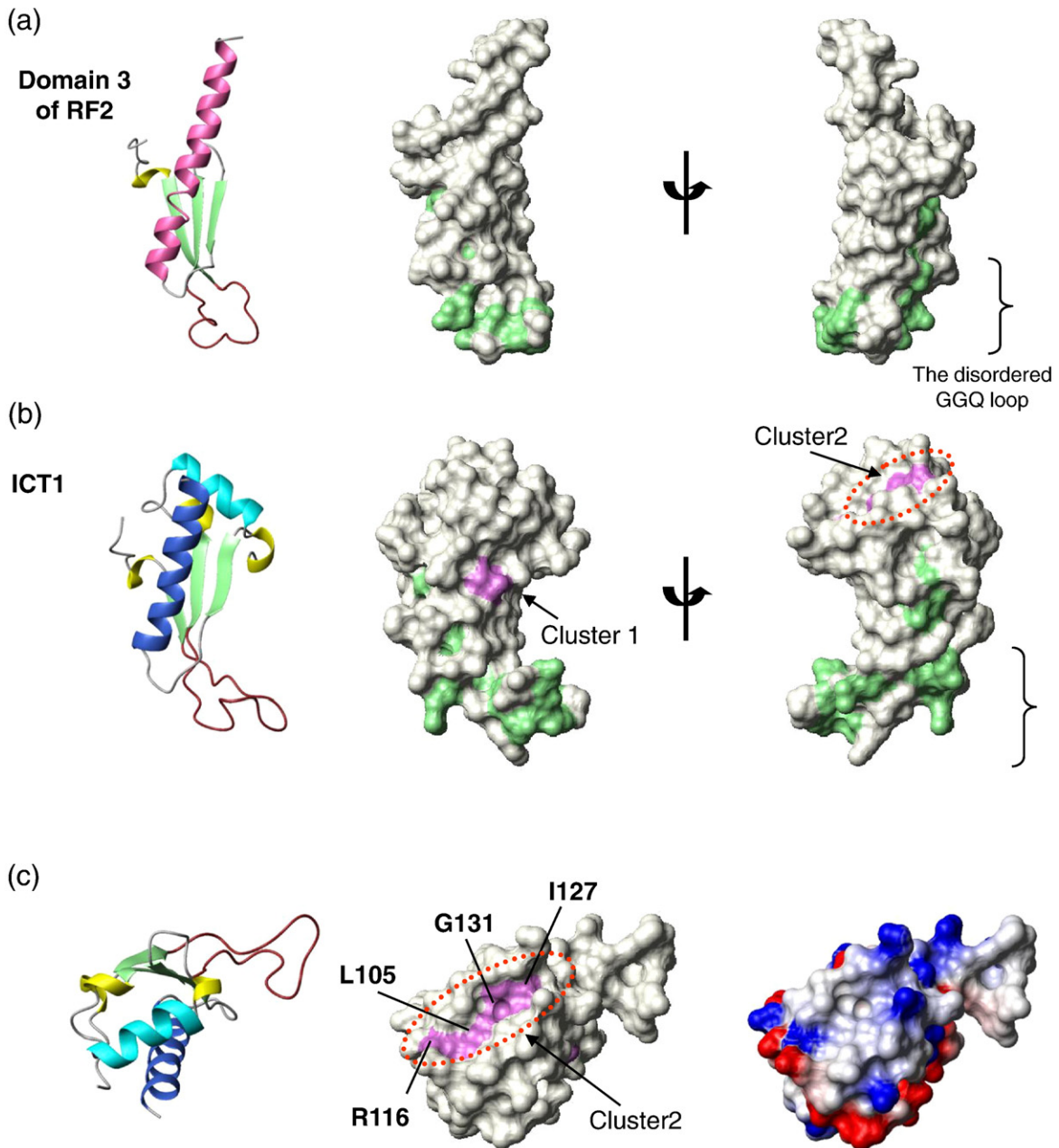
Fig. 6. Surface representations of the catalytic domain structure of the ICT1 protein and the RF domain 3 structure showing the side chains of highly conserved residues. Ribbon diagram (left) and surface representations (middle and left) of the RF domain 3 structure (a) and the ICT1 structure (residues 69–162) (b). The images on the left and in the middle are in the same orientation. Highly conserved residues among all of the ICT1 proteins from bacteria and eukaryotes and the bacterial-type RFs (>94%; indicated by asterisks in Fig. 1c) are depicted in light green. Highly conserved residues among all ICT1 proteins from bacteria and eukaryotes (indicated by # in Fig. 1c) are depicted in purple. Cluster 2 is indicated by an orange dotted line, as described in the text. Note that the GGQ loops are disordered in both structures and, thus, their shapes vary. (c) Ribbon diagram (left) and surface representation (middle) of the ICT1 structure showing the characteristics of cluster 2 and the surface representation (right) of the electrostatic potential (blue, positive; red, negative) calculated by MOLMOL.[22]

be divided into three regions. The first region is an N-terminal region that functions as an import signal into mitochondria in eukaryotes, but not in bacteria.

The second region is a catalytic domain that forms a structure with a β1–β2–α1–β3–α2 topology and has PTH activity via the GGQ motif. The last region is a

C-terminal basic-residue-rich region that is presumably unstructured (Fig. 1a and c). Structure-based alignment indicated that both this domain architecture of the ICT1 protein and the catalytic domain structure are highly conserved among bacteria and eukaryotes (Fig. 1c), suggesting the universality of ICT1 function, as described below in all organisms.

Structural comparison showed significant similarities between the structural framework of the catalytic domain of ICT1 and the structural framework of domain 3 of bacterial-type RFs. However, although the two structures have the same PTH activity, the two proteins have different roles. To obtain insights into putative functional residues, we mapped highly conserved residues among all known ICT1 proteins and RFs from various organisms onto the ICT1 structures and identified surface clusters that may play a functional role. Figure 6 shows that common conserved residues between ICT1 proteins and RFs concentrate on the structured half of the ICT1 structure comprising the well-fit region and the GGQ loop. According to RF function, these residues contribute to PTH activity.[16,17] These similarities in sequence and structure suggest that, like RFs, ICT1 can directly enter the A-site of the large ribosomal subunit to interact with the PTC.

In contrast, in the other half not containing the well-fit region and the GGQ loop, we found differences that may be key elements for discriminating between the role of ICT1 and the role of RFs. The most characteristic feature is the presence of a connecting region between β2 and β3, containing α1, 3_{10}-2, and 3_{10}-3, which is unique to ICT1 proteins (Figs. 3 and 7). As a result, the other half of the structure is larger than that of domain 3 of RF2 (Fig. 6a and b). No common residues between all of the ICT1 proteins and bacterial-type RFs were found on the surfaces of the other half (Fig. 6b). Instead, two clusters of ICT1-specifc conserved residues were found on the surface of the ICT1 structure (Fig. 6b and c). Cluster 1 is composed of Leu135 in β3 and Lys153 in α2, and cluster 2 is composed of Leu105 in 3_{10}-2, Arg116 in α1, and Ile127 and Gly131 in the linking region between 3_{10}-3 and β3. In cluster 2, a groove is formed between α2 and the β-sheet, more specifically by the loop of β2–(3_{10}-2)–α1–(3_{10}-3)–β3. Interestingly, the groove is surrounded by negatively charged residues (Figs. 6c and 7) and may be a site of interaction with protein and/or RNA in the ribosome. These differences are most likely linked to an ICT1-specific function different from that of RFs.

At the C-terminal region, instead of a structured domain that recognizes the stop codon in RFs, ICT1 always has a characteristic basic-residue-rich region composed of ~20 residues, following the last α-helix α2 (Fig. 1a and c). This basic-residue-rich region and α2 are usually separated by several proline residues (Fig. 1c). Presumably because of the high basic residue content, this region is unstructured or flexible. This
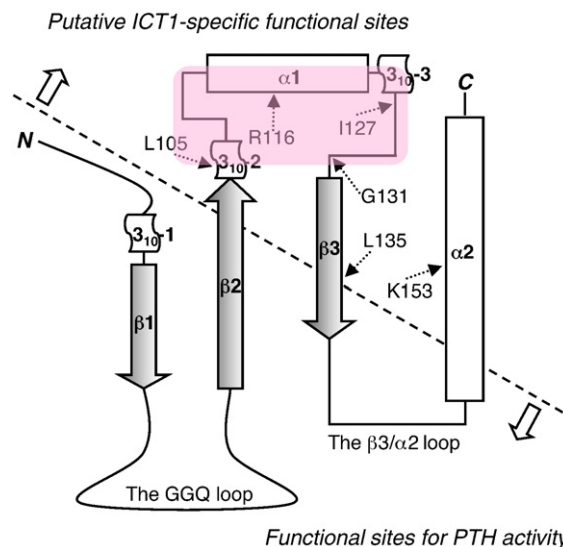

Fig. 7. Topology of the catalytic domain structure of the ICT1 protein showing functional sites and highly conserved residues among ICT1 proteins. Shown are the conserved residues among ICT1 proteins in Figs. 1c and 6b and c. The purple region indicates the groove formed by the cluster 2 residues shown in Fig. 6c. The broken line separates the topology into two parts based on their functional sites.

C-terminal region is reminiscent of some ribosomal proteins such as S17. Only when S17 binds to the 30S subunit does the flexible C-terminal extension become helical and wedged in 16S RNA.[23] Since ICT1 is a component of the mitoribosome,[10] the C-terminal region would become structured and functional when bound to the ribosome.

The lack of ICT1 in HeLa cells inhibited cell proliferation. FCM analysis showed that inhibition is due to cell cycle arrest and that cell death is apoptotic. In addition, FCM analysis showed decreases in both mitochondrial membrane potential and mass, and cytochrome *c* oxidase activity was impaired. These findings indicate that ICT1 is essential for cell vitality and mitochondrial function. A recent study has shown that the lack of ICT1 reduces translational efficiency in mitochondria.[10] Accordingly, it is thought that subunits of respiratory complexes coding for 13 genes (in mammals) of mitochondrial DNA cannot be synthesized sufficiently to make an adequate electrochemical proton gradient across the inner membranes. Accumulation of these defective mitochondria would lead to apoptosis.[24] Decreases in mitochondrial membrane potential and mitochondrial mass are often observed as an early event of apoptosis.[25,26]

It was found that mitochondrial protein synthesis requires ICT1 function, although the detailed role of ICT1 is unclear. The codon-independent PTH activity suggests that ICT1 rescues ribosomes that are

stalled for various reasons, such as truncated mRNA lacking a stop codon.[10] Considering that ICT1 is associated with ribosomes,[10] during normal translation elongation and termination, ICT1 is thought to be positioned away from the A-site so as not to disturb the entry of aminoacyl-tRNAs or RFs. Only when a ribosome is stalled can the position of ICT1 be altered to enter the A-site of the stalled ribosome to hydrolyze a peptidyl-tRNA at the P-site like RFs. Possibly, the C-terminal extension is fixed as an anchor, and the catalytic domain is movable. In addition, there arise questions on how ICT1 bound to ribosome discriminates a prematurely terminated peptidyl-tRNA on a stalled ribosome from a normal peptidyl-tRNA on ribosomes during translation and how ICT1 interacts with the PTC in a codon-independent manner. The characteristic features of the ICT1 protein revealed in this study seem to play key roles in this process on the ribosome. Further studies will be required to elucidate not only the exact function of ICT1 but also all aspects of the mitochondrial translation apparatus.

Materials and Methods

Sequence alignment data

Sequence alignments were performed with the CLUSTAL W program[27] and then manually modified based on ICT1 and RF structures. Accession codes used in sequence alignments are indicated in parentheses: *Mus musculus* ICT1 (NP_081005), *Homo sapiens* ICT1 (Q14197), *Monodelphis domestica* ICT1 (XP_001377961), *Taeniopygia guttata* ICT1 (XP_002190739), *Xenopus tropicalis* ICT1 (AAL67705), *Danio rerio* ICT1 (XP_001922710), *Drosophila melanogaster* ICT1 (NP_609416), *Pupulas trichocapa* ICT1 (PT12985), *Saccharomyces cerevisiae* ICT1 (Q12322), *E. coli* ICT1 (P40711), *Salmonella typhimurium* ICT1 (NP_459245), *Pseudomonas aeruginosa* ICT1 (NP_249559), *Zymomonas mobilis* ICT1 (CAA63804), *Chlorobium tepidum* ICT1 (NP_662859), *Streptomyces avermitilis* ICT1 (NP_825123), *Prochlorococcus marinus* ICT1 (NP_896036), *Synechocystis* sp. ICT1 (NP_942271), *E. coli* RF2 (P07012), *E. coli* RF1 (P07011), *Thermus thermophilus* RF2 (AAS82194.1), *H. sapiens* mtRF1a (NP_061914), *M. musculus* mtRF1 (Q8K126), *D. melanogaster* mtRF1 (NP_609617), *S. cerevisiae* mtRF1 (P30775).

Protein expression and purification

The DNA encoding the region of the ICT1 protein ranging from Glu63 to Ser162 was subcloned by PCR from a mouse full-length cDNA clone with the NIA mouse clone H3024H01.[28,29] This DNA fragment was cloned into the expression vector pCR2.1 (Invitrogen) as a fusion with an N-terminal 6-His affinity tag and a tobacco etch virus protease cleavage site. The $^{13}C/^{15}N$-labeled fusion protein was synthesized by the cell-free protein expression system, as described previously.[11,12,30] The solution was first adsorbed to a HiTrap Chelating column (Amersham Biosciences), which was washed with buffer A [50 mM

sodium phosphate buffer (pH 8.0) containing 500 mM sodium chloride and 20 mM imidazole] and eluted with buffer B [50 mM sodium phosphate buffer (pH 8.0) containing 500 mM sodium chloride and 500 mM imidazole]. To remove the His tag, we incubated the eluted protein with the tobacco etch virus protease at 4 °C overnight. After dialysis against buffer A without imidazole, the dialysate was mixed with imidazole to a final concentration of 20 mM and then applied to a HiTrap Chelating column, which was washed with buffer A. The flow-through fraction was dialyzed against buffer C [20 mM sodium phosphate buffer (pH 6.2) containing 0.1 mM PMSF and 1 mM DTT]. The dialysate was applied to a HiTrap SP column with a concentration gradient of buffers C and D [20 mM sodium phosphate buffer (pH 6.2) containing 1 M sodium chloride, 0.1 mM PMSF, and 1 mM DTT]. The ICT1-containing fractions were collected.

For NMR measurements, the purified protein was concentrated to ~1.7 mM in $^1H_2O/^2H_2O$ (9:1), 20 mM sodium phosphate buffer (pH 6.0), 100 mM NaCl, 1 mM 1,4-DL-dithiothreitol-d_{10} (*d*-DTT), and 0.02% NaN$_3$.

NMR spectroscopy, structure determination, and structure analysis

All NMR measurements were performed on Bruker AVANCE 600 and AVANCE 800 spectrometers at 25 °C. Sequence-specific backbone chemical shift assignments[31] were made with the $^{13}C/^{15}N$-labeled sample using standard triple-resonance experiments.[32,33] Assignments of side chains were obtained from HBHA(CO)NH, HC(CO) NH, C(CO)NH, HC(C)H total correlated spectroscopy, and HC (C)H-COSY spectra. ^{15}N-edited and ^{13}C-edited NOE spectroscopy spectra with mixing times of 80 ms were used to determine the distance restraints. The spectra were processed with the program NMRPipe.[34] The program KUJIRA, which was created based on NMRView,[35] was employed for optimal visualization and spectral analysis.[36]

Automated NOE cross-peak assignments[14] and structure calculations with torsion angle dynamics[13] were performed using the software package CYANA 1.0.7.[37] Peak lists of the two NOE spectroscopy spectra were generated as input with the program NMRView.[35] The input further contained the chemical shift list corresponding to sequence-specific assignments. Dihedral angle restraints were derived using the program TALOS.[38] No hydrogen bond restraints were used.

A total of 100 conformers were independently calculated. The 20 conformers of CYANA cycle 7 with the lowest final CYANA target function values were energy-minimized in a water shell with the program OPALp,[39] using AMBER force field.[40] The structures were validated using PROCHECK-NMR.[41] The program MOLMOL was used to analyze the resulting 20 conformers and to prepare drawings of the structures.[22]

Cell culture and transfection

HeLa cells were maintained in Dulbecco's modified Eagle's medium (DMEM) supplemented with 10% fetal bovine serum (FBS), 2 mM glutamine, 100 U/ml penicillin, and 100 μg/ml streptomycin (GPS). These cells were transfected with siRNAs using HilyMax (Dojindo).

Preparation of siRNA and transfection

The siRNA sequence used for the targeted silencing of ICT1 was chosen as described by B-Bridge International, Inc., and as recommended by Hokkaido System Science. The corresponding target mRNA sequences for the siRNAs were as follows:

si-ICT1-A: GCACUGAGUUCAAGAGCAU;
si-ICT1-B: GCAGAUUGCCUGCAGAAAA;
si-ICT1-C: CGGGAAAGGCUGAGACAAA.

The corresponding nontarget mRNA sequences for the siRNAs were as follows:

Nontarget-A: AUCCGCGCGAUAGUACGUA;
Nontarget-B: UUACGCGUAGCGUAAUACG;
Nontarget-C: UAUUCGCGCGUAUAGCGGU.

The concentration of siRNAs was 0.25 nM during transfections, which were facilitated by HilyMax, also according to the protocol of Hokkaido System Science.

Immunoblot assay

HeLa cells were harvested and lysed in ice-cold lysis buffer (7 M urea, 2 M thiourea, and 1% Triton X-100). The total protein concentrations of the lysate were determined using the Quick Start Bradford Dye Reagent (Bio-Rad). The proteins (50 μg/lane) were separated on a 15% SDS-PAGE and subsequently transferred to a nitrocellulose membrane. The membrane was blocked with 1% nonfat dried milk in phosphate-buffered saline (PBS) containing 0.2% polyoxyethylene (20) sorbitan monolaurate (Tween 20) at room temperature for 1 h before being incubated with human ICT1 polyclonal antibody (1:500, anti-mouse; Abnoba) and horseradish-peroxidase-conjugated anti-mouse immunoglobulin G (1:4000; Cell Signaling Technology). The protein was visualized by SuperSignal West Pico Chemiluminescent Substrate (Thermo Fisher Scientific). The blots were also probed with a human monoclonal γ-tubulin antibody (1:4000, anti-mouse; Sigma) as control for loading.

Cell concentration

Viability was determined over the course of the experiment by comparing serial dilutions of the stains using trypan blue staining. For trypan blue staining, 30 μl of the culture was combined with 120 μl of 0.4% trypan blue solution (Wako). The ratio of viable cells to inviable cells was determined by counting cells with a hemocytometer.

DNA content per cell cycle analysis

About 0.5×10^5 HeLa cells were plated in 35-mm culture dishes, collected using trypsin–ethylenediaminetetraacetic acid (EDTA), resuspended in DMEM without FBS, washed with PBS, and fixed in a solution of 70% ethanol at -20 °C overnight. Fixed cells were centrifuged at 1500 rpm and washed twice with PBS. DNA content was determined in a solution containing 2.0 mg/ml ribonuclease A (Qiagen) at 37 °C for 2 h. The cells were stained with PI (Wako) for 10 min in the dark, and the PI-elicited fluorescence of individual cells was measured by FCM using FACSCalibur (Becton Dickinson), with laser excitation at 488 nm and emissions of >590 nm collected in a linear-scale fashion. We analyzed a total of 10^4 cells for each sample and determined the percentages of the cell cycle.

Annexin V–fluorescein isothiocyanate/PI assay

To identify apoptotic cells, we stained the cells with PI and fluorescein isothiocyanate (FITC)-conjugated Annexin V using the Annexin V–FITC Apoptosis Detection Kit I (Becton Dickinson). Annexin V indicates early apoptotic cells based on externalized phosphatidylserine. PI detects cells that have lost plasma membrane integrity (i.e., necrotic or late apoptotic cells). HeLa cells were harvested using trypsin–EDTA, washed with PBS, resuspended in 500 μl of binding buffer supplemented with 5 μl of Annexin V–FITC and 5 μl of PI solution, and treated in the dark for 5 min at room temperature. After the addition of binding buffer, the stained cells were kept on ice and analyzed by FCM. We collected the FITC fluorescence between 515 nm and 545 nm and the PI fluorescence between 564 nm and 606 nm. A total of 10^4 cells per sample were measured in each experiment.

Fluorescent detection of mitochondrial membrane potential

The membrane-potential-dependent stain MitoTracker Red CMXRos (Molecular Probes) was used to assess mitochondrial membrane potential in HeLa cells. The cells were incubated in media containing a 0.1 μM final concentration of MitoTracker Red CMXRos for 20 min at 37 °C in a 5% CO_2 gas incubator. The cells were collected using trypsin–EDTA, resuspended in DMEM without FBS, suspended with 1 ml of PBS, and fixed in a solution of 4% paraformaldehyde for 10 min at 4 °C. The cells were analyzed by FCM.

Mitochondrial mass analysis

The mitochondria mass per cell was measured by FCM using MitoTracker Green FM (Molecular Probes). HeLa cells were collected by trypsinization, suspended in 1 ml of PBS, and stained with 100 nM MitoTracker Green FM for 30 min at room temperature in the dark.

Cytochrome *c* oxidase assay

Cytochrome *c* oxidase assay was conducted using the Mitochondria Isolation Kit for Cultured Cells (Pierce) and the Cytochrome *c* Oxidase Activity Assay Kit (BioChain) in accordance with the manufacturers' instructions.

Protein Data Bank accession numbers

The sequence-specific resonance assignments of ICT1 have been deposited in BioMagResBank (accession number 10121). The atomic coordinates of the 20 energy-minimized CYANA conformers of the mouse ICT1 protein have been deposited in RCSB Protein Data Bank (PDB) under PDB code 1J26.

Acknowledgements

Supplementary Data

Supplementary data to this article can be found online at doi:10.1016/j.jmb.2010.09.033

References

1. van Belzen, N., Diesveld, M. P., van der Made, A. C., Nozawa, Y., Dinjens, W. N., Vlietstra, R. *et al.* (1995). Identification of mRNAs that show modulated expression during colon carcinoma cell differentiation. *Eur. J. Biochem.* **234**, 843–848.

2. van Belzen, N., Dinjens, W. N., Eussen, B. H. & Bosman, F. T. (1998). Expression of differentiation-related genes in colorectal cancer: possible implications for prognosis. *Histol. Histopathol.* **13**, 1233–1242.

3. Finn, R. D., Mistry, J., Tate, J., Coggill, P. C., Heger, A., Pollington, J. E. *et al.* (2010). The Pfam protein families database. *Nucleic Acids Res.* **38**, D211–D222.

4. Klaholz, B. P., Pape, T., Zavialov, A. V., Myasnikov, A. G., Orlova, E. V., Vestergaard, B. *et al.* (2003). Structure of the *Escherichia coli* ribosomal termination complex with release factor 2. *Nature*, **421**, 90–94.

5. Rawat, U. B., Zavialov, A. V., Sengupta, J., Valle, M., Grassucci, R. A., Linde, J. *et al.* (2003). A cryo-electron microscopic study of ribosome-bound termination factor RF2. *Nature*, **421**, 87–90.

6. Zavialov, A. V., Mora, L., Buckingham, R. H. & Ehrenberg, M. (2002). Release of peptide promoted by the GGQ motif of class 1 release factors regulates the GTPase activity of RF3. *Mol. Cell*, **10**, 789–798.

7. Frolova, L. Y., Tsivkovskii, R. Y., Sivolobova, G. F., Oparina, N. Y., Serpinsky, O. I., Blinov, V. M. *et al.* (1999). Mutations in the highly conserved GGQ motif of class 1 polypeptide release factors abolish ability of human eRF1 to trigger peptidyl-tRNA hydrolysis. *RNA*, **5**, 1014–1020.

8. Kumar, A., Agarwal, S., Heyman, J. A., Matson, S., Heidtman, M., Piccirillo, S. *et al.* (2002). Subcellular localization of the yeast proteome. *Genes Dev.* **16**, 707–719.

9. Pagliarini, D. J., Calvo, S. E., Chang, B., Sheth, S. A., Vafai, S. B., Ong, S. E. *et al.* (2008). A mitochondrial protein compendium elucidates complex I disease biology. *Cell*, **134**, 112–123.

10. Richter, R., Rorbach, J., Pajak, A., Smith, P. M., Wessels, H. J., Huynen, M. A. *et al.* (2010). A functional peptidyl-tRNA hydrolase, ICT1, has been recruited into the human mitochondrial ribosome. *EMBO J.* **29**, 1116–1125.

11. Kigawa, T., Yabuki, T., Matsuda, N., Matsuda, T., Nakajima, R., Tanaka, A. & Yokoyama, S. (2004). Preparation of *Escherichia coli* cell extract for highly productive cell-free protein expression. *J. Struct. Funct. Genomics*, **5**, 63–68.

12. Kigawa, T., Yabuki, T., Yoshida, Y., Tsutsui, M., Ito, Y., Shibata, T. & Yokoyama, S. (1999). Cell-free production and stable-isotope labeling of milligram quantities of proteins. *FEBS Lett.* **442**, 15–19.

13. Gütert, P., Mumenthaler, C. & Wührich, K. (1997). Torsion angle dynamics for NMR structure calculation with the new program DYANA. *J. Mol. Biol.* **273**, 283–298.

14. Herrmann, T., Gütert, P. & Wührich, K. (2002). Protein NMR structure determination with automated NOE-identification in the NOESY spectra using the new software ATNOS. *J. Biomol. NMR*, **24**, 171–189.

15. Vestergaard, B., Van, L. B., Andersen, G. R., Nyborg, J., Buckingham, R. H. & Kjeldgaard, M. (2001). Bacterial polypeptide release factor RF2 is structurally distinct from eukaryotic eRF1. *Mol. Cell*, **8**, 1375–1382.

16. Laurberg, M., Asahara, H., Korostelev, A., Zhu, J., Trakhanov, S. & Noller, H. F. (2008). Structural basis for translation termination on the 70S ribosome. *Nature*, **454**, 852–857.

17. Weixlbaumer, A., Jin, H., Neubauer, C., Voorhees, R. M., Petry, S., Kelley, A. C. & Ramakrishnan, V. (2008). Insights into translational termination from the structure of RF2 bound to the ribosome. *Science*, **322**, 953–956.

18. Trobro, S. & Aqvist, J. (2009). Mechanism of the translation termination reaction on the ribosome. *Biochemistry*, **48**, 11296–11303.

19. Vermes, I., Haanen, C. & Reutelingsperger, C. (2000). Flow cytometry of apoptotic cell death. *J. Immunol. Methods*, **243**, 167–190.

20. Pacheco, T. R., Moita, L. F., Gomes, A. Q., Hacohen, N. & Carmo-Fonseca, M. (2006). RNA interference knockdown of hU2AF[35] impairs cell cycle progression and modulates alternative splicing of Cdc25 transcripts. *Mol. Biol. Cell*, **17**, 4187–4199.

21. Tondera, D., Santel, A., Schwarzer, R., Dames, S., Giese, K., Klippel, A. & Kaufmann, J. (2004). Knockdown of MTP18, a novel phosphatidylinositol 3-kinase-dependent protein, affects mitochondrial morphology and induces apoptosis. *J. Biol. Chem.* **279**, 31544–31555.

22. Koradi, R., Billeter, M. & Wührich, K. (1996). MOLMOL: a program for display and analysis of macromolecular structures. *J. Mol. Graphics*, **14**, 51–55.

23. Brodersen, D. E., Clemons, W. M., Jr., Carter, A. P., Wimberly, B. T. & Ramakrishnan, V. (2002). Crystal structure of the 30S ribosomal subunit from *Thermus thermophilus*: structure of the proteins and their interactions with 16S RNA. *J. Mol. Biol.* **316**, 725–768.

24. Ventura-Clapier, R., Garnier, A. & Veksler, V. (2008). Transcriptional control of mitochondrial biogenesis: the central role of PGC-1α. *Cardiovasc. Res.* **79**, 208–217.

25. Ly, J. D., Grubb, D. R. & Lawen, A. (2003). The mitochondrial membrane potential ($\Delta\psi_m$) in apoptosis; an update. *Apoptosis*, **8**, 115–128.

26. Lugli, E., Troiano, L., Ferraresi, R., Roat, E., Prada, N., Nasi, M. *et al.* (2005). Characterization of cells with different mitochondrial membrane potential during apoptosis. *Cytometry Part A*, **68**, 28–35.

27. Thompson, J. D., Higgins, D. G. & Gibson, T. J. (1994). CLUSTAL W: improving the sensitivity of progressive multiple sequence alignment through sequence weighting, position-specific gap penalties and weight matrix choice. *Nucleic Acids Res.* **22**, 4673–4680.

28. Kargul, G. J., Dudekula, D. B., Qian, Y., Lim, M. K., Jaradat, S. A., Tanaka, T. S. *et al.* (2001). Verification and initial annotation of the NIA mouse 15K cDNA clone set. *Nat. Genet.* **28**, 17–18.

29. Tanaka, T. S., Jaradat, S. A., Lim, M. K., Kargul, G. J., Wang, X., Grahovac, M. J. *et al.* (2000). Genome-wide expression profiling of mid-gestation placenta and embryo using a 15,000 mouse developmental cDNA microarray. *Proc. Natl Acad. Sci. USA*, **97**, 9127–9132.

30. Kigawa, T. (2010). Cell-free protein production system with the *E. coli* crude extract for determination of protein folds. *Methods Mol. Biol.* **607**, 101–111.

31. Wührich, K. (1986). *NMR of Proteins and Nucleic Acids.* John Wiley and Sons, Inc., New York, NY.

32. Bax, A. (1994). Multidimensional nuclear magnetic resonance methods for protein studies. *Curr. Opin. Struct. Biol.* **4**, 738–744.

33. Cavanagh, J., Fairbrother, W. J., Palmer, A. G. & Skelton, N. J. (1996). *Protein NMR Spectroscopy, Principles and Practice.* Academic Press, Inc., San Diego, CA.

34. Delaglio, F., Grzesiek, S., Vuister, G. W., Zhu, G., Pfeifer, J. & Bax, A. (1995). NMRPipe: a multidimensional spectral processing system based on UNIX pipes. *J. Biomol. NMR*, **6**, 277–293.

35. Johnson, B. & Blevins, R. (1994). NMRView: a computer program for the visualization and analysis of NMR data. *J. Biomol. NMR*, **4**, 603–614.

36. Kobayashi, N., Iwahara, J., Koshiba, S., Tomizawa, T., Tochio, N., Güntert, P. *et al.* (2007). KUJIRA, a package of integrated modules for systematic and interactive analysis of NMR data directed to high-throughput NMR structure studies. *J. Biomol. NMR*, **39**, 31–52.

37. Gütert, P. (2003). Automated NMR protein structure calculation. *Prog. NMR Spectrosc.* **43**, 105–125.

38. Cornilescu, G., Delaglio, F. & Bax, A. (1999). Protein backbone angle restraints from searching a database for chemical shift and sequence homology. *J. Biomol. NMR*, **13**, 289–302.

39. Koradi, R., Billeter, M. & Gütert, P. (2000). Point-centered domain decomposition for parallel molecular dynamics simulation. *Comput. Phys. Commun.* **124**, 139–147.

40. Cornell, W. D., Cieplak, P., Bayly, C. I., Gould, I. R., Merz, K. M., Ferguson, D. M. *et al.* (1995). A second generation force field for the simulation of proteins, nucleic acids, and organic molecules. *J. Am. Chem. Soc.* **117**, 5179–5197.

41. Laskowski, R. A., Rullmannn, J. A., MacArthur, M. W., Kaptein, R. & Thornton, J. M. (1996). AQUA and PROCHECK-NMR: programs for checking the quality of protein structures solved by NMR. *J. Biomol. NMR*, **8**, 477–486.